Supplementary Information

Theoretical design of durable and strong polycarbonate against photodegradation

Xiao Huang,[a] Yuuichi Orimoto,[b] and Yuriko Aoki [b,*]

[a]Department of Interdisciplinary Engineering Sciences, Chemistry and Materials Science, Interdisciplinary Graduate School of Engineering Sciences, Kyushu University, 6-1 Kasuga-Park, Fukuoka 816-8580, Japan.

[b]Department of Material Sciences, Faculty of Engineering Sciences, Kyushu University, 6-1 Kasuga-Park, Fukuoka 816-8580, Japan

*E-mail: aoki.yuriko.397@m.kyushu-u.ac.jp.

Table of Contents

1. Computational Details

In this work, the models (see Fig. 2) with one substituent at -$C(CH_3)_2$-*meta* position on each phenyl ring were chosen to study the substituent effect on carbonate PhO–COO bond. There are two reasons for the selection: (1) it may exist a large steric hindrance between the substituents and -$C(CH_3)_2$- group when the substituents locate at -$C(CH_3)_2$-*ortho* position, and (2) the PhO–COO bond cleavage does not occur when the -$C(CH_3)_2$-*meta* positions are occupied by two substituents[S1]. To examine the suitability of the functionals and basis sets, we used different functionals and basis sets to do the spectrum calculations of BPAHC based on the GS geometry (optimized using B3LYP/6-31G(d) method). Besides, we used B3LYP functional with different basis sets to do the GS and ES geometry optimization and the spectrum calculations for BPAHC. The corresponding results were displayed in Figs. S1-S5 and Tables S1-S3. CYLview[S2] software was used to depict the optimized geometries. Multiwfn 3.8[S3] and Origin 9.1[S4] software were utilized to plot the absorption spectra which were convoluted with a Gaussian function using a full width at half maximum of 0.38 eV. All calculations were performed by using Gaussian 16[S5] program.

2. Additional Figures and Tables

2.1 Absorption spectra and transition features (predicted by different functionals with 6-31G(d) basis set) of BPAHC based on the S_0 geometry (optimized using B3LYP/6-31G(d) method)

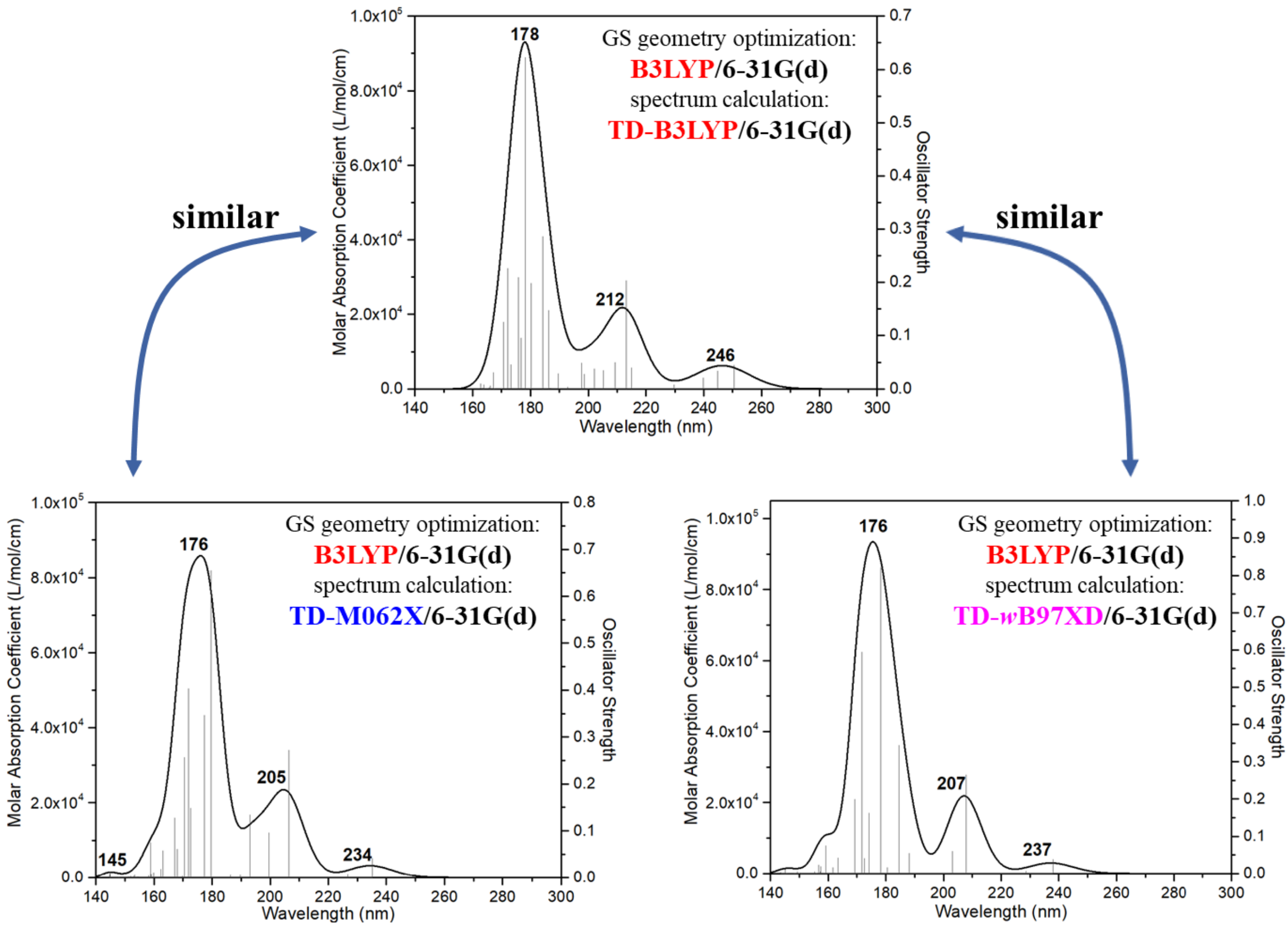

Fig. S1 Predicted absorption spectra by different functionals with 6-31G(d) basis set for BPAHC based on the S_0 geometry (optimized using B3LYP/6-31G(d)).

To examine the feasibility of the used functional B3LYP, the other two different functionals M062X[S6] and *w*B97XD[S7] were used to do the TDDFT calculations for BPAHC. As shown in Fig. S1, relative to the absorption spectrum of BPAHC using TD-B3LYP method, the peak positions and absorption intensities of spectra have small differences using TD-M062X and TD-*w*B97XD methods. These small variations of peak positions and absorption intensities of spectra indicate that B3LYP may be reasonable to do the spectra calculations for this study.

Table S1. Predicted main parameters by different functionals with 6-31G(d) basis set for the vertical excitation (UV-Vis absorption) of BPAHC based on the S_0 geometry (optimized using B3LYP/6-31G(d)).

Functionals	Electronic transition	Energy (eV)	λ (nm)	*f*[a]	Contributions	Assignment
B3LYP	$S_0 \rightarrow S_{13}$	6.54	190	0.0294	41.2%	$n_{(O\ of\ CO3)} \rightarrow \pi^*_{(Ph2)}$
					17.5%	$n_{(O\ of\ CO3)} \rightarrow \pi^*_{(CO3)}$
					15.1%	$\pi_{(Ph2)} \rightarrow \pi^*_{(Ph2)}$
M062X	$S_0 \rightarrow S_7$	6.65	186	0.0053	15.9%	$n_{(O\ of\ CO3)} \rightarrow \pi^*_{(Ph2)}$
					53.1%	$n_{(O\ of\ CO3)} \rightarrow \pi^*_{(CO3)}$
*w*B97XD	$S_0 \rightarrow S_7$	6.87	180	0.0156	23.5%	$n_{(O\ of\ CO3)} \rightarrow \pi^*_{(Ph2)}$
					55.0%	$n_{(O\ of\ CO3)} \rightarrow \pi^*_{(CO3)}$
					4.2%	$\pi_{(Ph2)} \rightarrow \pi^*_{(Ph2)}$

[a]Oscillator strength.

As displayed in Table S1, the $S_0 \rightarrow S_{13}$ transition using TD-B3LYP/6-31G(d) method corresponds to the $S_0 \rightarrow S_7$ transitions using TD-M062X/6-31G(d) and TD-*w*B97XD/6-31G(d), respectively. Same as the results using TD-B3LYP/6-31G(d) method, it also includes the electronic transitions to $\pi^*_{(Ph2)}$ orbital ($n_{(O\ of\ CO3)} \rightarrow \pi^*_{(Ph2)}$ and $\pi_{(Ph2)} \rightarrow \pi^*_{(Ph2)}$) and to $\pi^*_{(CO3)}$ orbital ($n_{(O\ of\ CO3)} \rightarrow \pi^*_{(CO3)}$) using the TD-M062X/6-31G(d) and TD-*w*B97XD/6-31G(d) methods. However, different from the results using TD-B3LYP/6-31G(d) method, the dominant transition becomes the $n_{(O\ of\ CO3)} \rightarrow \pi^*_{(CO3)}$ transition from the $n_{(O\ of\ CO3)} \rightarrow \pi^*_{(Ph2)}$ transition. Besides, relative to the results using TD-B3LYP/6-31G(d) method, the excitation energy and oscillator strength also vary using TD-M062X/6-31G(d) and TD-*w*B97XD/6-31G(d) methods. These differences may be because these three different functionals have the different HF components, B3LYP (20%), M062X (54%), and *w*B97XD (short range: 22.2%, long range: 100%). For example, M062X functional may overestimate the excitation energy due to the high HF component (54%), and the range-separated functional *w*B97XD also may overestimate the excitation energy due to the high HF component of long range (100%). Relatively, B3LYP functional with 20% HF component has slightly larger deviation in the excitation energy. These results of benchmarks are shown in the following paper[S10] (*Phys. Chem. Chem. Phys.*, 2011, 13, 16987-16998). Therefore, B3LYP functional may be suitable to do the calculations of vertical excitation for the studied models at the initial step of analysis.

In a word, B3LYP functional may be adequate to do the spectra calculations and discuss the concentrated transitions based on the above results.

2.2 Absorption spectra and transition features (predicted by TD-B3LYP with different basis sets) of BPAHC based on the S_0 geometry (optimized using B3LYP/6-31G(d) method)

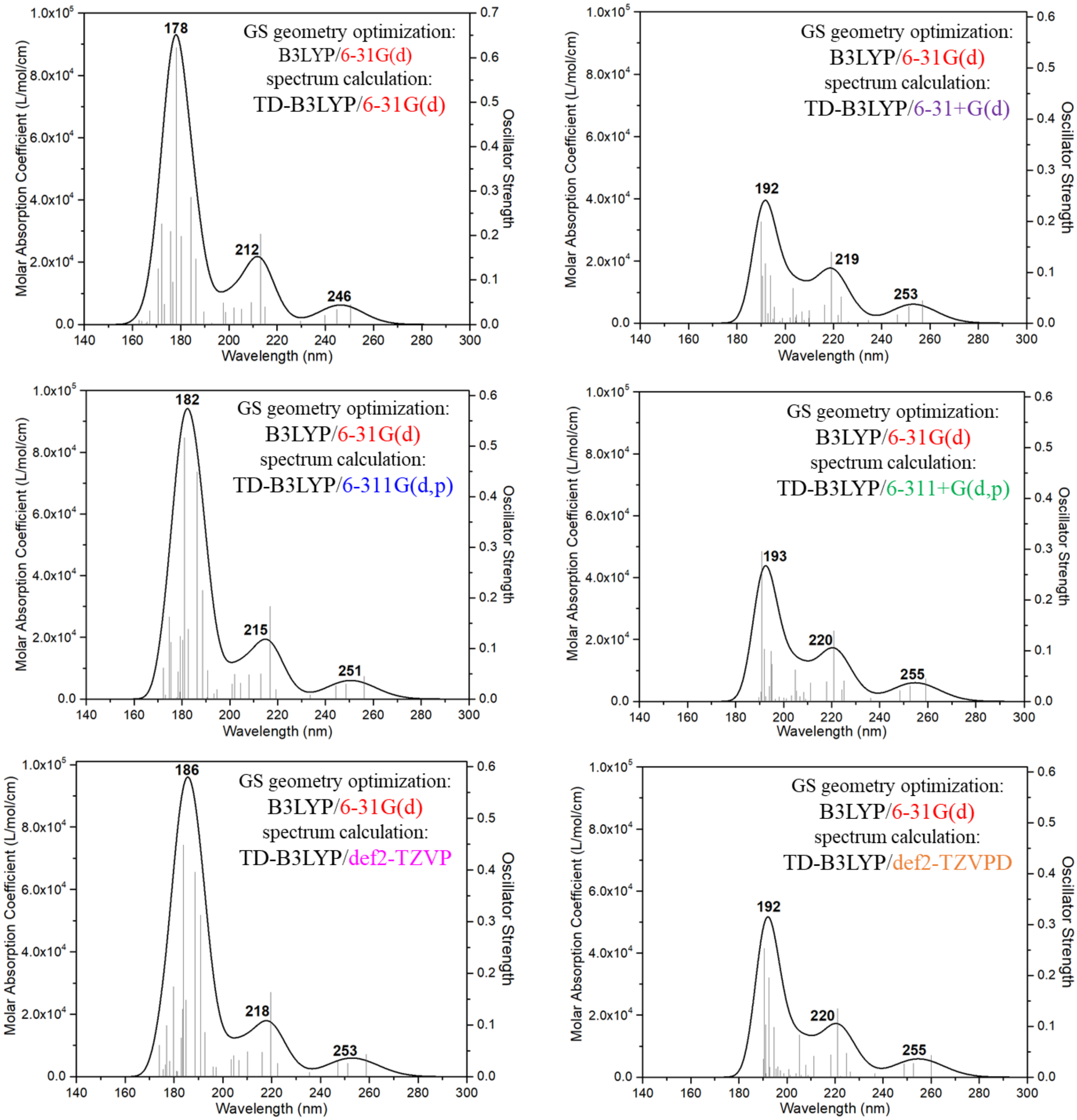

Fig. S2 Predicted absorption spectra by TD-B3LYP with different basis sets for BPAHC based on the S_0 geometry (optimized using B3LYP/6-31G(d) method).

Table S2. Predicted main parameters by TD-B3LYP with different basis sets for the vertical excitation (UV-Vis absorption) of BPAHC based on the S_0 geometry (optimized using B3LYP/6-31G(d) method).

Basis sets		Electronic transition	Energy (eV)	λ (nm)	f^a	Contributions	Assignment
without diffusion functions	6-31G(d)	$S_0 \rightarrow S_{13}$	6.54	190	0.0294	41.2%	$n_{(O\ of\ CO3)} \rightarrow \pi^*_{(Ph2)}$
						17.5%	$n_{(O\ of\ CO3)} \rightarrow \pi^*_{(CO3)}$
						15.1%	$\pi_{(Ph2)} \rightarrow \pi^*_{(Ph2)}$
	6-311G(d,p)	$S_0 \rightarrow S_{15}$	6.50	191	0.0568	29.0%	$n_{(O\ of\ CO3)} \rightarrow \pi^*_{(Ph2)}$
						9.0%	$n_{(O\ of\ CO3)} \rightarrow \pi^*_{(CO3)}$
						23.5%	$\pi_{(Ph2)} \rightarrow \pi^*_{(Ph2)}$
	def2-TZVP[S8]	$S_0 \rightarrow S_{16}$	6.44	193	0.0861	13.1%	$n_{(O\ of\ CO3)} \rightarrow \pi^*_{(Ph2)}$
						5.6%	$n_{(O\ of\ CO3)} \rightarrow \pi^*_{(CO3)}$
						32.0%	$\pi_{(Ph2)} \rightarrow \pi^*_{(Ph2)}$
with diffusion functions	6-31+G(d)	$S_0 \rightarrow S_{25}$	6.39	194	0.0946	7.2%	$n_{(O\ of\ CO3)} \rightarrow \pi^*_{(Ph2)}$
						3.0%	$n_{(O\ of\ CO3)} \rightarrow \pi^*_{(CO3)}$
						31.6%	$\pi_{(Ph2)} \rightarrow \pi^*_{(Ph2)}$
	6-311G+(d,p)	$S_0 \rightarrow S_{24}$	6.37	195	0.0995	5.9%	$n_{(O\ of\ CO3)} \rightarrow \pi^*_{(Ph2)}$
						2.8%	$n_{(O\ of\ CO3)} \rightarrow \pi^*_{(CO3)}$
						19.7%	$\pi_{(Ph2)} \rightarrow \pi^*_{(Ph2)}$
	def2-TZVPD[S9]	$S_0 \rightarrow S_{24}$	6.37	195	0.0985	9.0%	$n_{(O\ of\ CO3)} \rightarrow \pi^*_{(Ph2)}$
						3.5%	$n_{(O\ of\ CO3)} \rightarrow \pi^*_{(CO3)}$
						32.2%	$\pi_{(Ph2)} \rightarrow \pi^*_{(Ph2)}$

[a]Oscillator strength.

To check the suitability of the used basis set 6-31G(d), TDDFT calculations were performed to compare the absorption spectra and the centered transition for BPAHC using different basis sets. As shown in Fig. S2, based on the S_0 geometry (optimized using B3LYP/6-31G(d) method), there are almost no change for the peak positions of absorption spectra using different basis sets with or without diffusion functions. However, when the basis sets with the diffusion function are used, the absorption intensity around 185 nm have a very large decrease compared to the cases without diffusion function. That means for the spectra calculations, the basis sets with diffusion function doesn't affect the peak positions of absorption spectra which are important during the discussions, only affects the absorption intensity which are difficult to obtain the accurate results through calculation in general. The almost no change of absorption peaks positions using different basis sets indicate that 6-31G(d) basis set may be sufficient to do the spectra calculations for the studied models in this work.

In this study, the $S_0 \rightarrow S_{13}$ transition (using TD-B3LYP/6-31G(d) method) based on the S_0 geometry (optimized using B3LYP/6-31G(d) method) was focused on to discuss the PC carbonate C–O bond cleavage, because it includes the electronic transitions to the carbonate π anti-bonding and to the phenyl group (adjacent to the carbonate group) π anti-bonding which are responsible for the carbonate C–O bond cleavage of BPAHC. To examine whether the used basis set 6-31G(d) is suitable or not, the additional basis sets using TD-B3LYP method are used to compare the corresponding transition features relative to that using TD-B3LYP/6-31G(d) method, which are shown in Table S2.

As displayed in Table S2, for the results of the basis sets without diffusion functions, the $S_0 \rightarrow S_{13}$ transition using 6-31G(d) basis set corresponds to $S_0 \rightarrow S_{15}$ transition using 6-311G(d,p) basis set, $S_0 \rightarrow S_{16}$ transition using def2-TZVP basis set, respectively. With the increase of the basis sets, the electronic transition to $\pi^*_{(Ph2)}$ orbital ($n_{(O\ of\ CO3)} \rightarrow \pi^*_{(Ph2)}$ and $\pi_{(Ph2)} \rightarrow \pi^*_{(Ph2)}$) increases and to $\pi^*_{(CO3)}$ orbital ($n_{(O\ of\ CO3)} \rightarrow \pi^*_{(CO3)}$) decreases, indicating that the size of basis set has an effect on the transition contributions. However, although the transition contributions have some changes using larger basis sets 6-311G(d,p) and def2-TZVP, the electronic transition to $\pi^*_{(Ph2)}$ orbital ($n_{(O\ of\ CO3)} \rightarrow \pi^*_{(Ph2)}$ and $\pi_{(Ph2)} \rightarrow \pi^*_{(Ph2)}$) is still the major transition and the electronic transition to $\pi^*_{(CO3)}$ orbital ($n_{(O\ of\ CO3)} \rightarrow \pi^*_{(CO3)}$) is the minor transition, which are in consistent with the transition contribution using small basis set 6-31G(d) qualitatively.

For the results of basis sets with diffusion functions displayed in Table S2, the $S_0 \rightarrow S_{13}$ transition using 6-31G(d) basis set corresponds to the $S_0 \rightarrow S_{25}$ transition using 6-31+G(d) basis set, $S_0 \rightarrow S_{24}$ transition using 6-311+G(d,p) basis set, and $S_0 \rightarrow S_{24}$ transition using def2-TZVPD basis set, respectively. Compared to the transition feature using TD-B3LYP/6-31G(d) method, for the corresponding transition contributions using these three basis sets with diffusion functions, the electronic transition to $\pi^*_{(Ph2)}$ orbital ($n_{(O\ of\ CO3)} \rightarrow \pi^*_{(Ph2)}$ and $\pi_{(Ph2)} \rightarrow \pi^*_{(Ph2)}$) is the major transition and the electronic transition to $\pi^*_{(CO3)}$ orbital ($n_{(O\ of\ CO3)} \rightarrow \pi^*_{(CO3)}$) is the minor transition, which are in consistent with the transition contribution using small basis set 6-31G(d) qualitatively.

Based on the above results, it can be seen that the B3LYP/6-31G(d) may produce the reasonable results for the studied models in this work.

2.3 BPAHC GS geometries (optimized using B3LYP with different basis sets) and ES geometries (optimized using TD-B3LYP with different basis sets); absorption spectra and transition features (predicted by TD-B3LYP with different basis sets) based on the GS geometries (optimized using B3LYP with different basis sets)

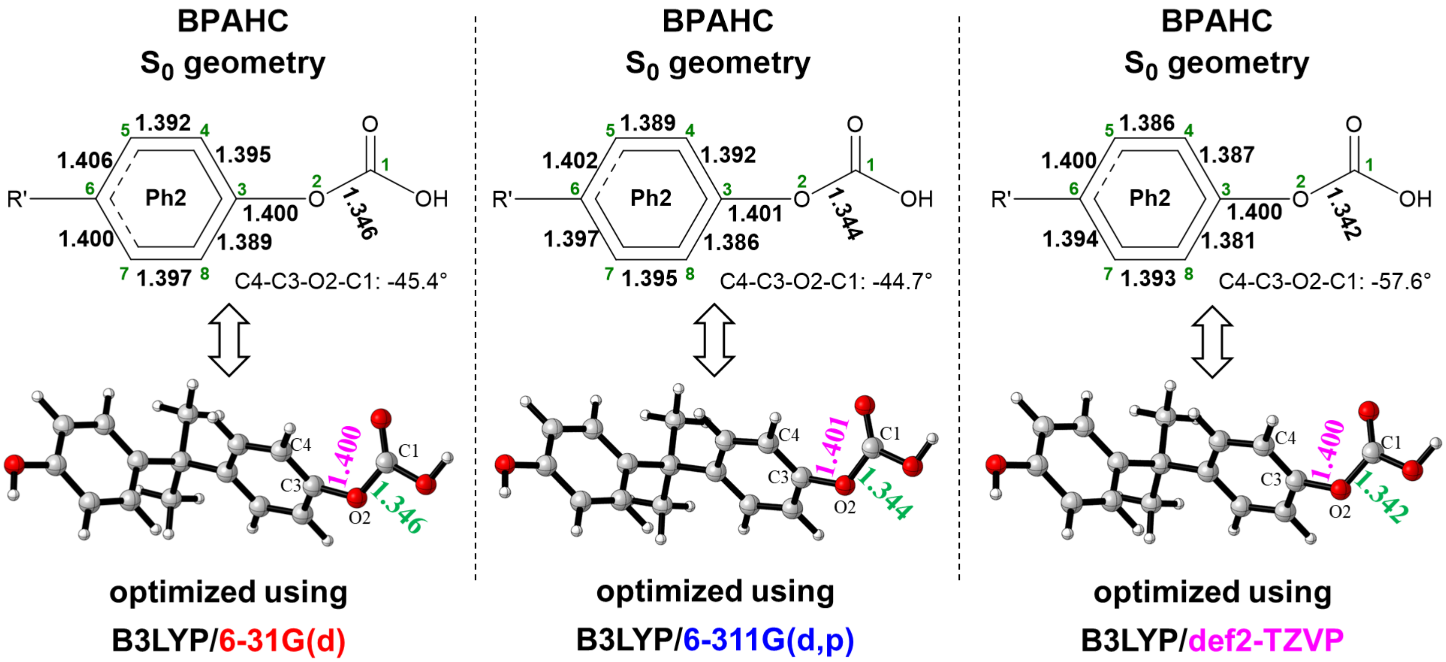

Fig. S3 Optimized GS geometries using B3LYP functional with different basis sets of BPAHC including the main bond lengths and dihedral angle. (R': HOPhC(CH_3)$_2$-)

To check whether the used basis set 6-31G(d) is suitable or not for the GS geometry optimization of the studied models, the other two larger basis sets 6-311G(d) and def2-TZVP were used to optimize the GS geometry of BPAHC. As shown in Fig. S3, the main bond distances of S_0 geometries (optimized using B3LYP with different basis sets) have very small differences. Relative to the dihedral angles of S_0 geometries using 6-31G(d) basis set, the C4-C3-O2-C1 dihedral angles have small distortions using 6-311G(d,p) basis set (about 1 degrees), while it has a relative large distortion using def2-TZVP basis set (about 10 degrees). These results indicate that the 6-31G(d) basis set may be sufficient for the GS geometry optimization.

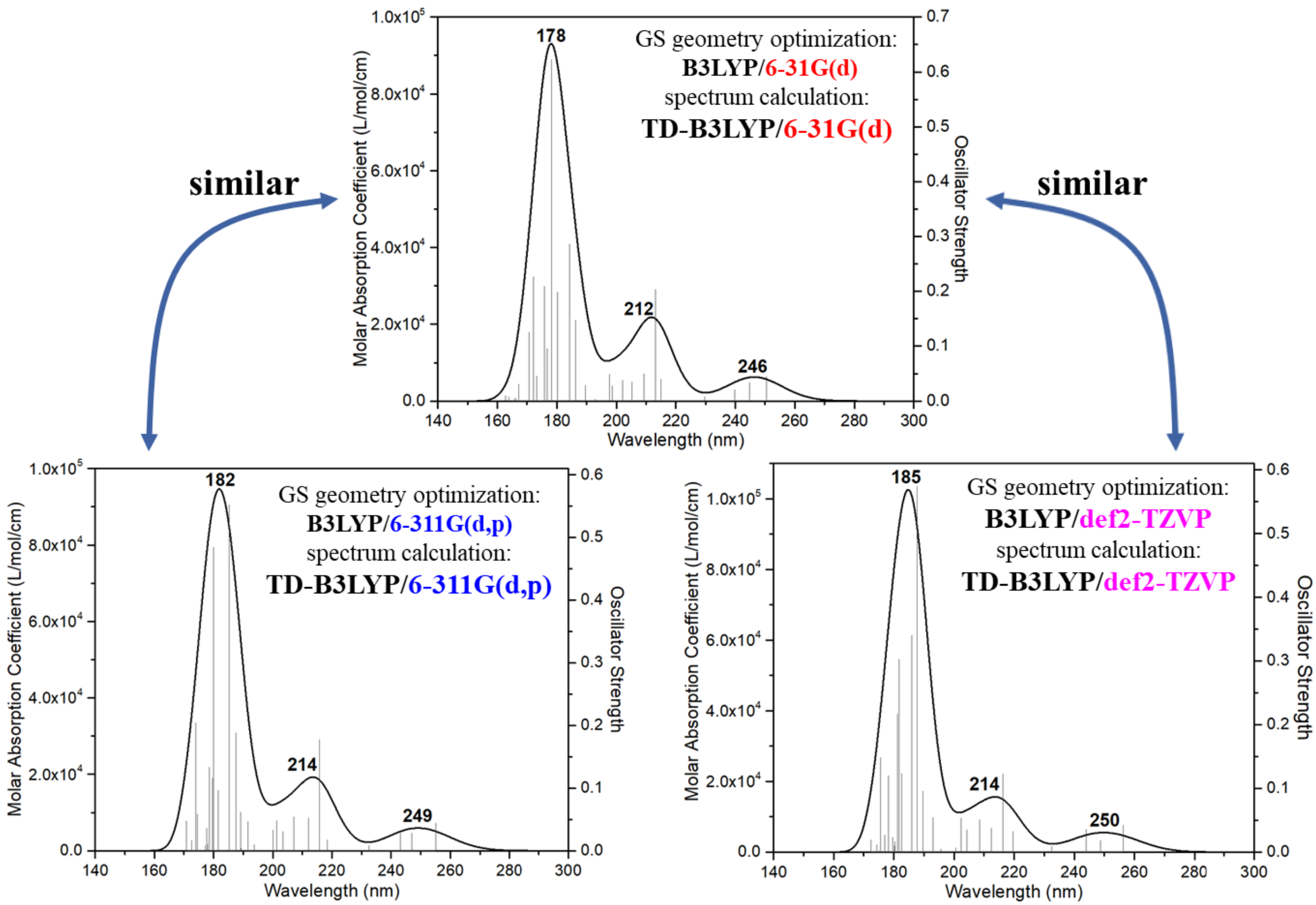

Fig. S4 Predicted absorption spectra by TD-B3LYP with different basis sets for BPAHC based on the GS geometries (optimized using the same functional B3LYP with different basis sets).

Table S3. Predicted transition features by TD-B3LYP with different basis sets for BPAHC based on the GS geometries (optimized using the same functional B3LYP with different basis sets).

Basis sets	Electronic transition	Energy (eV)	λ (nm)	f^a	Contributions	Assignment
6-31G(d)	$S_0 \rightarrow S_{13}$	6.54	190	0.0294	41.2%	$n_{(O\ of\ CO3)} \rightarrow \pi^*_{(Ph2)}$
					17.5%	$n_{(O\ of\ CO3)} \rightarrow \pi^*_{(CO3)}$
					15.1%	$\pi_{(Ph2)} \rightarrow \pi^*_{(Ph2)}$
6-311G(d,p)	$S_0 \rightarrow S_{19}$	6.83	182	0.0965	24.6%	$n_{(O\ of\ CO3)} \rightarrow \pi^*_{(Ph2)}$
					5.8%	$n_{(O\ of\ CO3)} \rightarrow \pi^*_{(CO3)}$
					11.8%	$\pi_{(Ph2)} \rightarrow \pi^*_{(Ph2)}$
def2-TZVP	$S_0 \rightarrow S_{17}$	6.60	188	0.5745	8.5%	$n_{(O\ of\ CO3)} \rightarrow \pi^*_{(Ph2)}$
					4.4%	$n_{(O\ of\ CO3)} \rightarrow \pi^*_{(CO3)}$
					25.5%	$\pi_{(Ph2)} \rightarrow \pi^*_{(Ph2)}$

[a]Oscillator strength.

Based on the above GS geometries (optimized using B3LYP functional with different basis sets), the absorption spectra and transition features (predicted by TD-B3LYP with different basis sets) of BPAHC were compared which are shown in Fig. S4 and Table S3.

In Fig. S4, for the absorption spectra (predicted by TD-B3LYP method with different basis sets) of BPAHC based on the GS geometries (optimized using B3LYP functional with different basis sets), the peak positions of spectra have small variations when using the different basis sets, indicating that it has a little effect on the absorption spectra of BPAHC even using the larger basis sets 6-311G(d,p) and def2-TZVP.

As displayed in Table S3, based on the GS geometries (optimized using B3LYP with different basis sets), the transition features (predicted by TD-B3LYP with different basis sets) of BPAHC were compared. The results show that the $S_0 \rightarrow S_{13}$ transition using 6-31G(d) basis set corresponds to the $S_0 \rightarrow S_{19}$ transition using 6-311G(d,p) basis set and the $S_0 \rightarrow S_{17}$ transition using def2-TZVP basis set, respectively. As the basis sets increase, the transition contributions of the electronic transition to $\pi^*_{(Ph2)}$ orbital ($n_{(O\ of\ CO3)} \rightarrow \pi^*_{(Ph2)}$ and $\pi_{(Ph2)} \rightarrow \pi^*_{(Ph2)}$) increases and to $\pi^*_{(CO3)}$ orbital ($n_{(O\ of\ CO3)} \rightarrow \pi^*_{(CO3)}$) decreases, indicating that the size of basis set can affect the transition contributions. However, although there are some changes of the transition contributions when using larger basis sets 6-311G(d,p) and def2-TZVP, the electronic transition to $\pi^*_{(Ph2)}$ orbital ($n_{(O\ of\ CO3)} \rightarrow \pi^*_{(Ph2)}$ and $\pi_{(Ph2)} \rightarrow \pi^*_{(Ph2)}$) is still dominant and the electronic transition to $\pi^*_{(CO3)}$ orbital ($n_{(O\ of\ CO3)} \rightarrow \pi^*_{(CO3)}$) is non-dominant, which are consistent with the transition contribution (predicted by TD-B3LYP with small basis set 6-31G(d)) qualitatively.

Based on the above results, it may be sufficient to do the spectra calculations and discuss the transition features (predicted by TD-B3LYP/6-31G(d) method) based on the GS geometry (optimized using B3LYP/6-31G(d) method) for the studied models in this work.

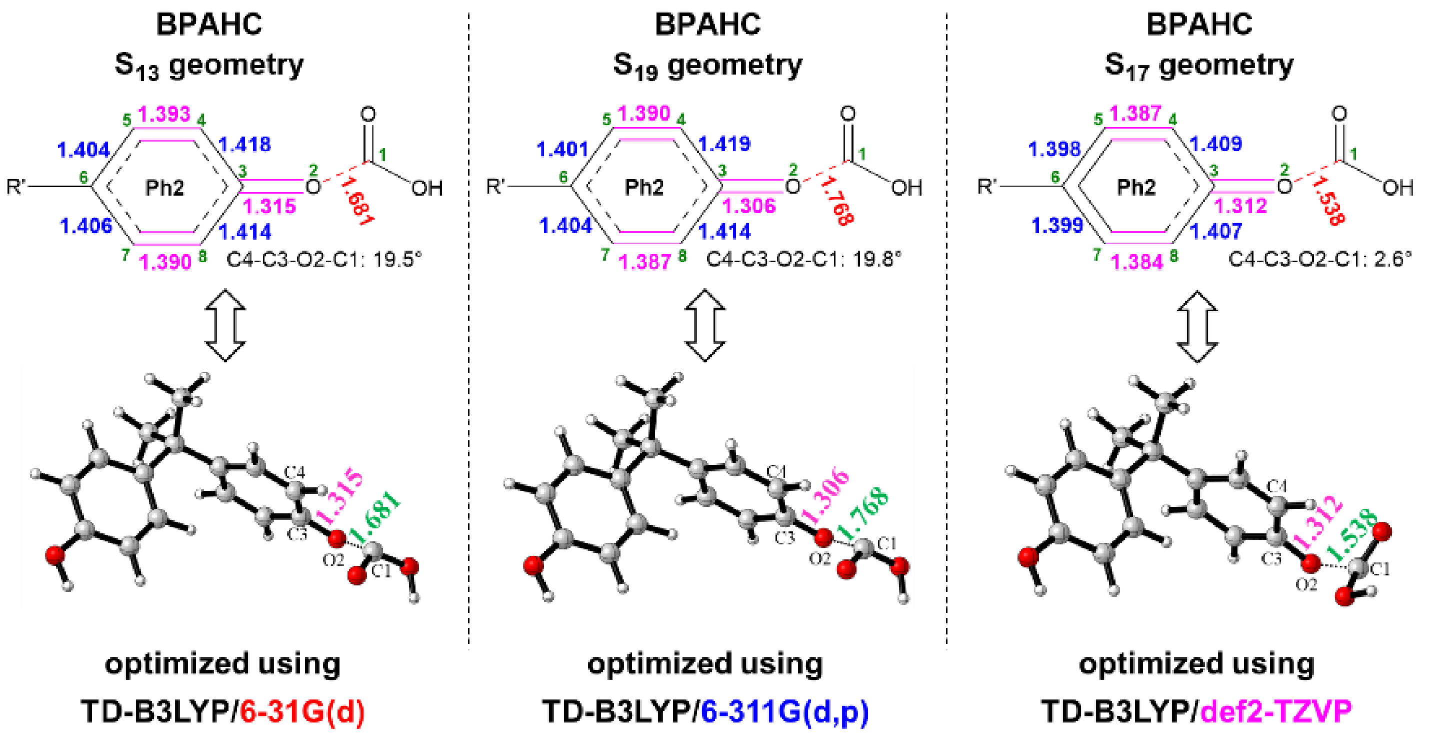

Fig. S5 Optimized ES geometries using TD-B3LYP method with different basis sets of BPAHC including the main bond lengths and dihedral angle. (R': HOPhC(CH_3)$_2$-)

Based on the transition features in the above Table S3, the corresponding ES geometries were optimized using TD-B3LYP/6-311G(d,p) (S_{19} geometry) and TD-B3LYP/def2-TZVP (S_{17} geometry), respectively. The comparison of the main bond lengths and dihedral angles of ES geometries (optimized using TD-B3LYP with different basis sets) of BPAHC is shown in Fig. S5.

As displayed Fig. S5, compared to the bond distances of ES geometry (S_{13} geometry, optimized using TD-B3LYP/6-31G(d) method), the O2–C1 bond distances have relatively large variations for S_{19} geometry (optimized using TD-B3LYP/6-311G(d,p) method) and S_{17} geometry (optimized using TD-B3LYP/def2-TZVP method). Except for the O2–C1 bond distance, the other bond distances have small differences among these three ES geometries which are optimized using TD-B3LYP with different basis sets. Relative to the dihedral angle of S_{13} geometry (optimized using TD-B3LYP/6-31G(d) method), it has a small distortion for S_{19} geometry (optimized using TD-B3LYP/6-311G(d,p) method), while it has a relatively large distortion within 20 degrees for S_{17} geometry (optimized using TD-B3LYP/def2-TZVP method). However, although the optimized ES geometries have some changes for O2–C1 bond distances and C4-C3-O2-C1 dihedral angles when using the larger basis sets, these three ES geometries optimized using TD-B3LYP with small or larger basis sets are prone to be the similar quinoid-like structure along the C6-C3-O2 line with C4=C5, C7=C8, and C3=O2 double bonds, finally breaking the carbonate O2–C1 bond. These results indicate that the TD-B3LYP method with small 6-31G(d) basis set may be sufficient to do the optimization of ES geometry for the studied models in this work.

In the view of the above results, the basis set 6-31G(d) may produce the reasonable GS and ES geometries, and absorption spectra for the studied models.

2.4 Absorption spectra and vertical parameters

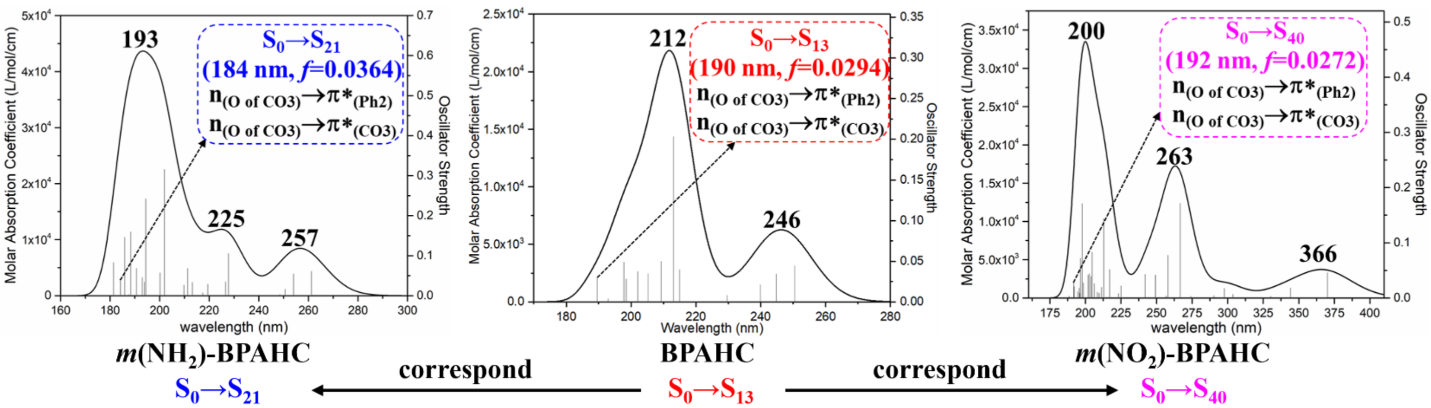

Fig. S6 Absorption spectra (at a longer wavelength of 180 nm) of BPAHC, *m*(NH_2)-BPAHC, and *m*(NO_2)-BPAHC based on their S_0 geometries predicted by TDDFT method. (*f*: oscillator strength)

Table S4 Vertical parameters related to the Ph2 and carbonate groups for BPAHC, *m*(NH_2)-BPAHC, and *m*(NO_2)-BPAHC based on their S_0 geometries (H: HOMO; L: LUMO. Ph-t: Ph1 and Ph2.)

	electronic transition	energy (eV)	λ (nm)	f^a	contribution (%)	transition	assignment
BPAHC	$S_0 \rightarrow S_{13}$	6.54	190	0.0294	41.2	H-4→L+1	$n_{(O\ of\ CO3)} \rightarrow \pi^*_{(Ph2)}$
					17.5	H-4→L+4	$n_{(O\ of\ CO3)} \rightarrow \pi^*_{(CO3)}$
					15.1	H-3→L+1	$\pi_{(Ph2)} \rightarrow \pi^*_{(Ph2)}$
					7.1	H-3→L+4	$\pi_{(Ph2)} \rightarrow \pi^*_{(CO3)}$
m(NH_2)-BPAHC	$S_0 \rightarrow S_{21}$	6.73	184	0.0364	36.5	H-5→L	$n_{(O\ of\ CO3)} \rightarrow \pi^*_{(Ph2)}$
					33.8	H-5→L+4	$n_{(O\ of\ CO3)} \rightarrow \pi^*_{(CO3)}$
					9.9	H-5→L+1	$n_{(O\ of\ CO3)} \rightarrow \pi^*_{(Ph1)}$
					3.9	H-5→L+3	$n_{(O\ of\ CO3)} \rightarrow \pi^*_{(Ph1)}$
					3.4	H-3→L+3	$\pi_{(Ph-t)} \rightarrow \pi^*_{(Ph1)}$
					2.8	H-5→L+2	$n_{(O\ of\ CO3)} \rightarrow \pi^*_{(Ph2)}$
m(NO_2)-BPAHC	$S_0 \rightarrow S_{40}$	6.46	192	0.0272	42.6	H-5→L+2	$n_{(O\ of\ CO3)} \rightarrow \pi^*_{(Ph2)}$
					2.1	H-5→L+6	$n_{(O\ of\ CO3)} \rightarrow \pi^*_{(CO3)}$
					4.1	H-1→L+4	$\pi_{(Ph2)} \rightarrow \pi^*_{(Ph2)}$
					2.3	H-2→L+2	$\pi_{(Ph2)} \rightarrow \pi^*_{(Ph2)}$
					24.3	H-13→L+1	$\pi_{(Ph1)} \rightarrow \pi^*_{(Ph2\ \&\ NO2)}$
					6.7	H-14→L+1	Mixed MO→$\pi^*_{(Ph2\ \&\ NO2)}$
					3.5	H-12→L+1	Mixed MO→$\pi^*_{(Ph2\ \&\ NO2)}$
					3.9	H-7→L+2	$p_{(O\ of\ NO2)} \rightarrow \pi^*_{(Ph2)}$

[a]Oscillator strength.

As shown in Fig. S6 and Table S4, $S_0 \rightarrow S_{21}$ transition in *m*(NH_2)-BPAHC and $S_0 \rightarrow S_{40}$ transition in *m*(NO_2)-BPAHC, corresponding to the $S_0 \rightarrow S_{13}$ transition of BPAHC, were chosen to discuss the substituent effect on carbonate O–C bond. Because both of them also have the excitations from carbonate oxygen lone pair to carbonate π anti-bonding and adjacent phenyl π anti-bonding. Besides, $S_0 \rightarrow S_{21}$ transition in *m*(NH_2)-BPAHC and $S_0 \rightarrow S_{40}$

transition in *m*(NO_2)-BPAHC have relatively large oscillator strengths of 0.0364 and 0.0272, respectively, similar to that of BPAHC (0.0294). This implies that they have relatively high contributions to the absorption spectra.

The absorption occurs at ca. 190 nm for the $S_0 \rightarrow S_{13}$ transition of BPAHC. Similarly, the absorptions are at ca. 184 nm and 192 nm for the $S_0 \rightarrow S_{21}$ transition in *m*(NH_2)-BPAHC and $S_0 \rightarrow S_{40}$ transition in *m*(NO_2)-BPAHC, respectively. The focused contributions of $S_0 \rightarrow S_{13}$ transition of BPAHC are H-4→L+1 (41.2%) and H-4→L+4 (17.5%), which correspond to H-5→L (36.5%) and H-5→L+4 (33.8%) for the $S_0 \rightarrow S_{21}$ transition of *m*(NH_2)-BPAHC, and correspond to H-5→L+2 (42.6%) and H-5→L+6 (2.1%) for the $S_0 \rightarrow S_{40}$ transition of *m*(NO_2)-BPAHC, respectively. They are assigned to $n_{(O\ of\ CO3)} \rightarrow \pi^*_{(Ph2)}$ and $n_{(O\ of\ CO3)} \rightarrow \pi^*_{(CO3)}$ as in BPAHC, respectively, indicating that $S_0 \rightarrow S_{21}$ transition of *m*(NH_2)-BPAHC and $S_0 \rightarrow S_{40}$ transition of *m*(NO_2)-BPAHC have a large effect on carbonate O–C bond. As for the $S_0 \rightarrow S_{40}$ transition of *m*(NO_2)-BPAHC, another excitation $\pi_{(Ph1)} \rightarrow \pi^*_{(Ph2\ \&\ NO2)}$ may also have a large effect on carbonate O–C bond because of a large transition contribution of 24.3%, which differs from the $S_0 \rightarrow S_{13}$ transition of BPAHC.

2.5 Optimized geometries of GS and ES (3D)

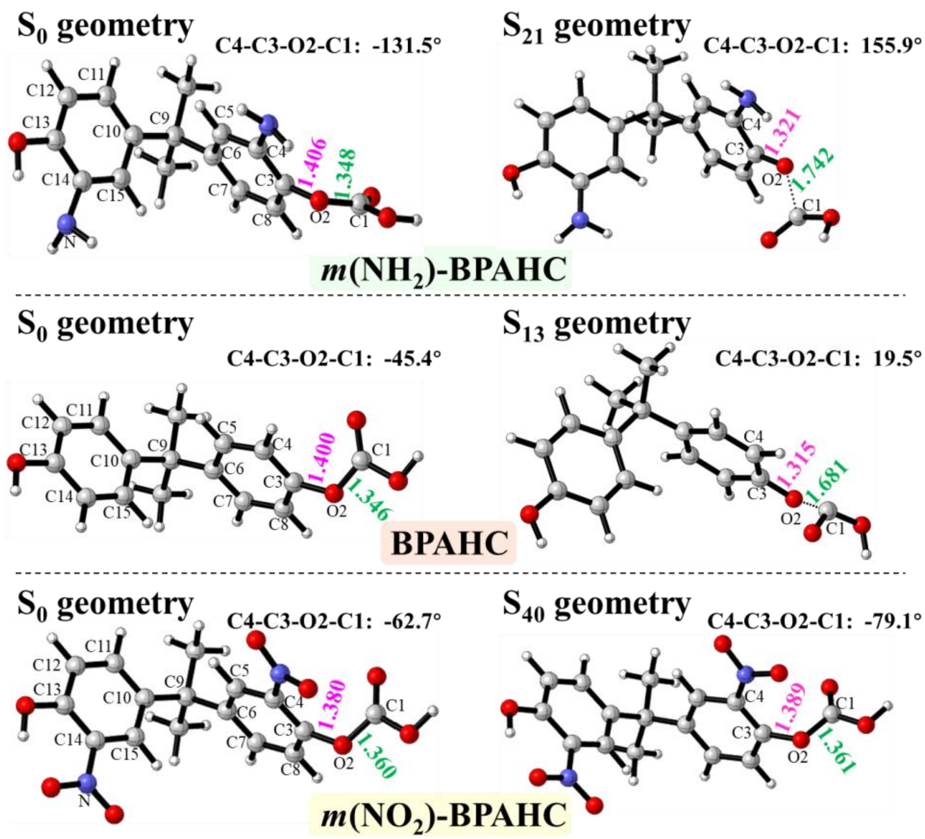

Fig. S7 Optimized geometries of GS and ES for BPAHC, *m*(NH_2)-BPAHC, and *m*(NO_2)-BPAHC.

To explore the geometric changes from the GS structure to the ES one, Fig. 4 shows the GS and ES geometries of the studied models including the main bond lengths of the carbonate and adjacent phenyl groups. Fig. S7 displays their 3D optimized geometries, corresponding to Fig. 4, for better understanding.

For BPAHC as shown in Fig. 4 center and Fig. S7 center, the C3–O2 and O2–C1 bond lengths are 1.400 Å and 1.346 Å in S_0 geometry, respectively, while the C3–O2 bond is shortened to 1.315 Å and the O2–C1 bond is extended to 1.681 Å in S_{13} geometry, indicating that upon excitation the C3–O2 bond has double bond nature and the O2–C1 bond is broken in S_{13} geometry. Similarly, for *m*(NH_2)-BPAHC (see Fig. 4 top and Fig. S7 top), the C3–O2 and O2–C1 bond lengths are 1.406 Å and 1.348 Å in S_0 geometry which exhibit the single bond nature, respectively, while they are 1.321 Å (C3–O2: having double bond nature) and 1.742 Å (O2–C1: being extended) in S_{21} geometry, respectively, implying the O2–C1 bond is destroyed in S_{21} geometry by excitation as in S_{13} geometry of BPAHC. The result reveals that the O2–C1 bond can be damaged even under the effect of -NH_2 substituent. Distinct from that of BPAHC, for *m*(NO_2)-BPAHC (see Fig. 4 bottom and Fig. S7 bottom) the C3–O2 bond length is similar in S_0 (1.380 Å) and S_{40} (1.389 Å) geometries, and the O2–C1 bond length is also similar in S_0 (1.360 Å) and S_{40} (1.361 Å) geometries, indicating that the C3–O2 and O2–C1 single bond natures are remained in S_{40} geometry relative to S_0 one. These results imply that the O2–C1 bond is not easy to be broken upon excitation affected by $-NO_2$ substituent.

With regard to the C4-C3-O2-C1 dihedral angle between the carbonate and adjacent phenyl groups, for BPAHC (see Fig. S7 center), it is -45.4º in S_0 geometry, and it becomes 19.5º in S_{13} geometry due to the separation of COOH moiety. For *m*(NH_2)-BPAHC (see Fig. S7 top), compared to that of S_0 geometry (-45.4º) in BPAHC, this dihedral angle (-131.5º) shows a large rotation of COOH moiety in S_0 geometry, indicating a large effect on this angle by $-NH_2$ substituent for S_0 geometry. It becomes 155.9º in S_{21} geometry relative to S_0 geometry of *m*(NH_2)-BPAHC because the carbonate plane is damaged upon excitation under the effect of $-NH_2$ substituent, which is the same situation as in BPAHC. However, for *m*(NO_2)-BPAHC (see Fig. S7 bottom), compared to that of S_0 geometry (-45.4º) in BPAHC, the C4-C3-O2-C1 dihedral angle (-62.7º) shows a relatively small rotation in S_0 geometry, implying that a little effect on this angle by $-NO_2$ group for S_0 geometry. It shows a slight rotation (-79.1º) in S_{40} geometry relative to S_0 geometry (-62.7º) of *m*(NO_2)-BPAHC since the carbonate group is maintained by excitation under the effect of $-NO_2$ substituent.

2.6 Another possible ES alternated structure of *m*(NO_2)-BPAHC

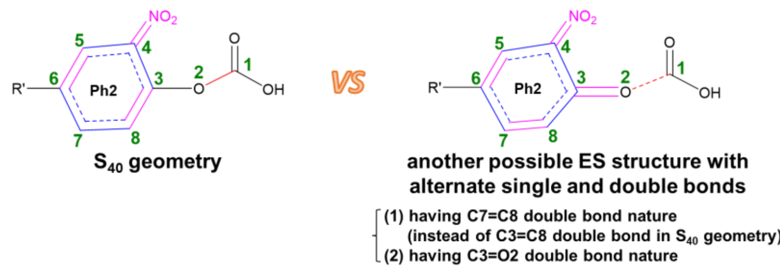

Fig. S8 S_{40} geometry and another possible ES structure with alternate bonds of *m*(NO_2)-BPAHC.

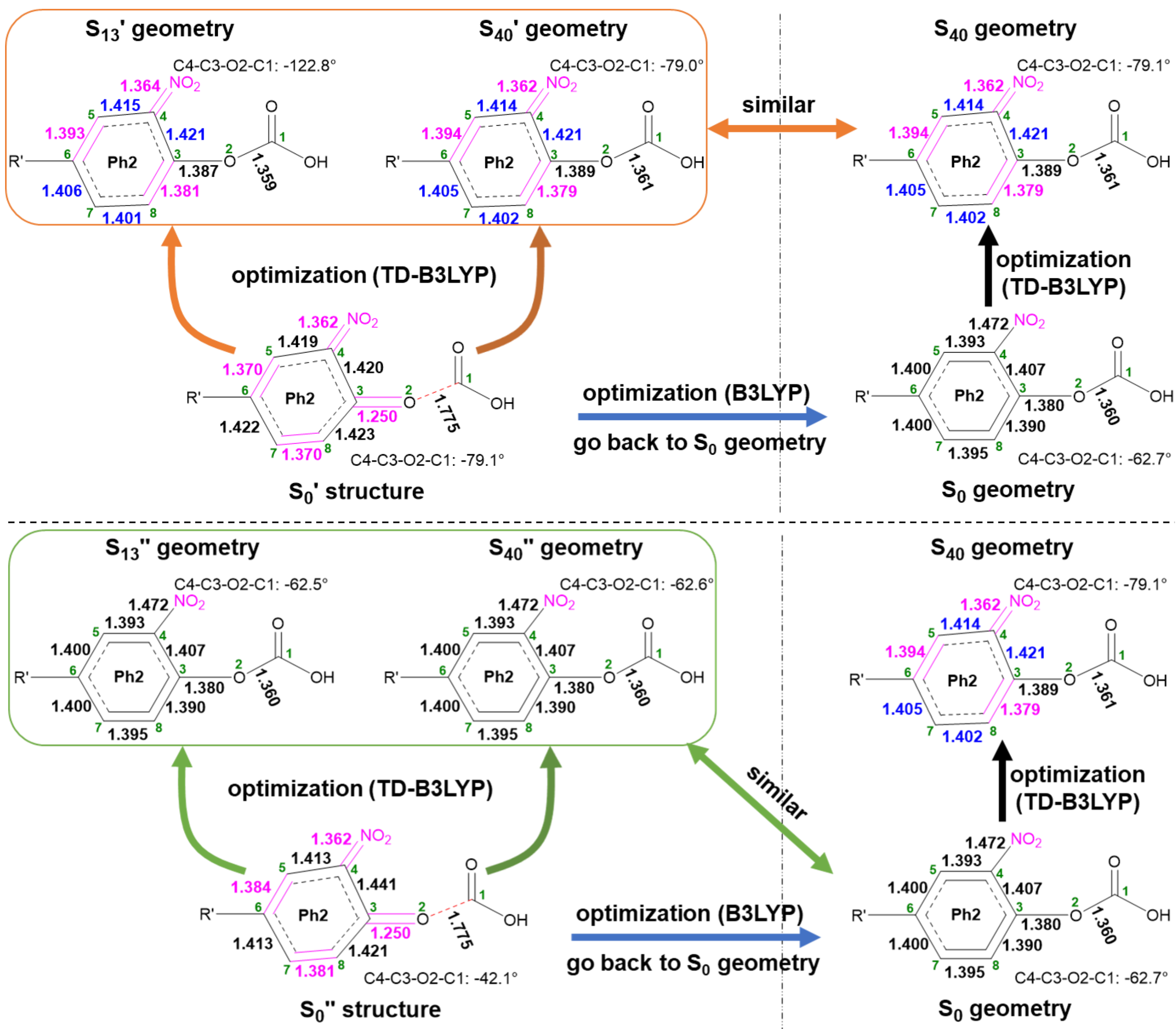

Fig. S9 Geometric comparisons of DFT and TDDFT optimized structures starting from different initial structures of *m*(NO_2)-BPAHC.

As shown in Fig. 4 center, S_{13} geometry of BPAHC has a quinoid-like structure which has C4=C5, C7=C8, and C3=O2 double bonds, finally cleaving the O2–C1 bond. However, S_{40} geometry (see Fig. 4 bottom and Fig. S8 left) of *m*(NO_2)-BPAHC has another different quinoid-like structure from that of BPAHC, with the C3=C8, C5=C6, and C4=NO_2 double bonds, which maintains the single bond nature for both the C3–O2 and O2–C1 bonds. Here, we confirmed the possibility of a similar quinoid-like ES structure (see Fig. S8 right) of *m*(NO_2)-BPAHC with C3=O2 double bond nature as in BPAHC, finally breaking the O2–C1 bond. For this purpose, the geometric comparisons were made starting from the different initial structures based on DFT and TDDFT calculations, and the results are shown in Fig. S9.

In Fig. S9 top, it can be seen that the S_{13}’ and S_{40}’ geometries that are similar to S_{40} geometry were obtained by TDDFT geometric optimizations even starting from S_0’ structure. Here, the S_0’ structure is a possible structure with alternate single and double bonds, and it is prepared according to the following bond lengths: (1) the C4–NO_2 bond length is set to be 1.362 Å as in S_{40} geometry, (2) the C–C bond lengths within Ph2 group are adjusted by hand based on the bond lengths of geometries in Fig. 4, (3) the C3–O2 bond is set to be 1.250 Å compared to the normal C=O double bond (1.230 Å), and (4) the O2–C1 bond is set to be 1.775 Å according to the O2–C1 bond length of S_{21} geometry in *m*(NH_2)-BPAHC. Then starting from the S_0’ structure, DFT and TDDFT calculations were performed, respectively. The S_{13}’ and S_{40}’ were chosen to be optimized when doing TDDFT optimization, because the S_0’→S_{13}’ and S_0’→S_{40}’ transitions based on S_0’ structure focus on the excitation to $\pi^*_{(CO3)}$ and $\pi^*_{(Ph2)}$ orbitals, where MO coefficients mainly concentrate on the carbonate and Ph2 groups. The results showed that TDDFT optimization starting from S_0’ structure leads to the S_{13}’ and S_{40}’ geometries similar to S_{40} geometry. On the other hand, the S_0’ structure went back to the S_0 geometry after DFT optimization, and to the S_{40} geometry after TDDFT optimization. These indicate that the S_0’ structure cannot be maintained in ES on its quinoid-like structure with C5=C6, C7=C8, and C3=O2 double bonds because it is not stable.

As shown in Fig. S9 bottom, S_0’’ structure is also a possible structure with alternate single and double bonds with slightly different parameters from the S_0’ structure. The S_0’’ structure was obtained by the partial optimization when fixing the O2–C1, C3=O2, and C4=NO_2 bonds of S_0’ structure, in order to keep C4=NO_2, C5=C6, C7=C8, and C3=O2 double bond natures in the S_0’’ structure. Due to the same reason as the above-mentioned, the S_{13}’’ and S_{40}’’ were chosen to be optimized based on TDDFT optimization. The results showed that the S_0’’ structure went back to the S_0 geometry regardless of DFT or TDDFT optimization, because the S_{13}’’ and S_{40}’’ structures by TDDFT optimization were equivalent to the S_0 geometry. This implies that the S_0’’ structure cannot be remained in ES because it is unstable, which is the same as the above-mentioned case.

In a word, even starting from the different initial structures S_0’ and S_0’’, another possible ES alternated structure of *m*(NO_2)-BPAHC cannot be obtained during the calculations because it is an unfavorable structure relative to the S_{40} geometry.

2.7 Three other different views of potential energy surfaces (PESs)

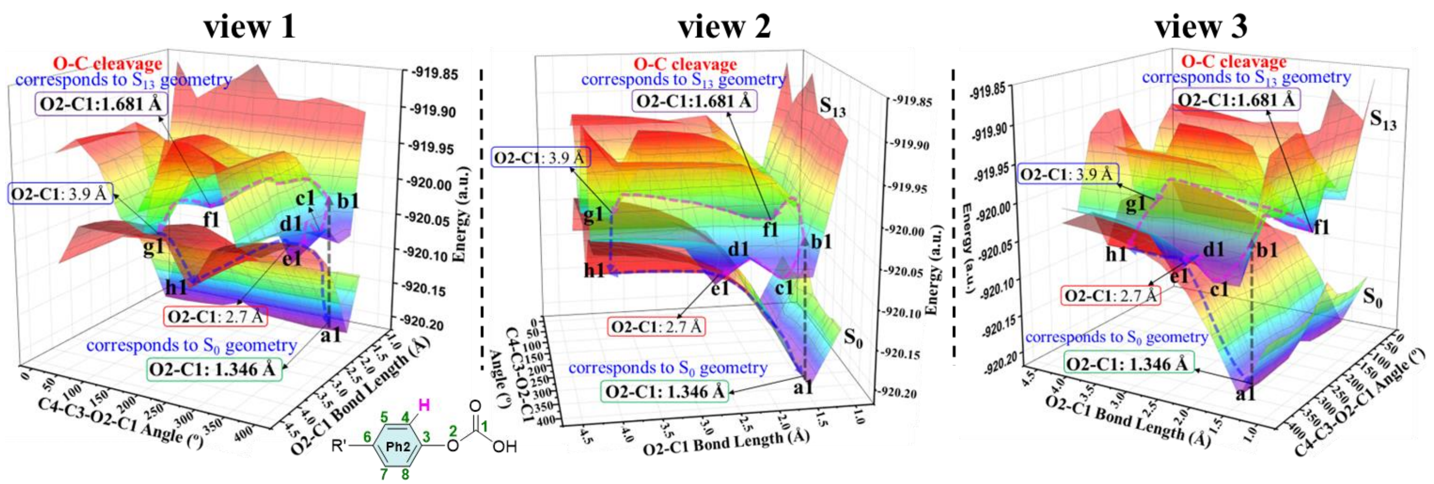

Fig. S10 Three different views of PES for BPAHC. (R'=HOPhC(CH_3)$_2$-)

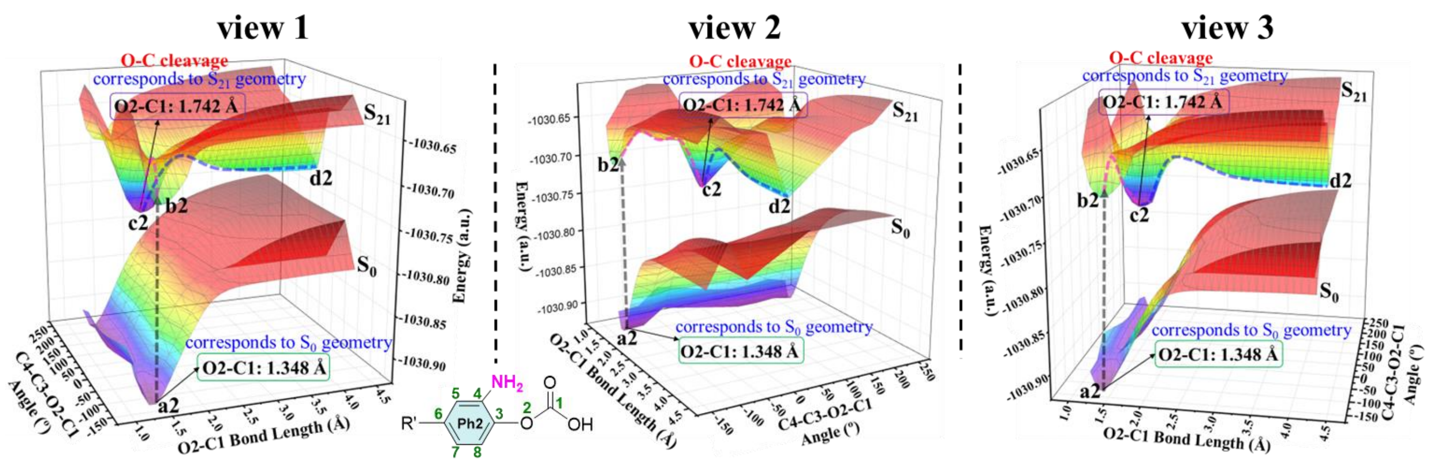

Fig. S11 Three different views of PES for *m*(NH_2)-BPAHC. (R'=HOPh(NH_2)C(CH_3)$_2$-)

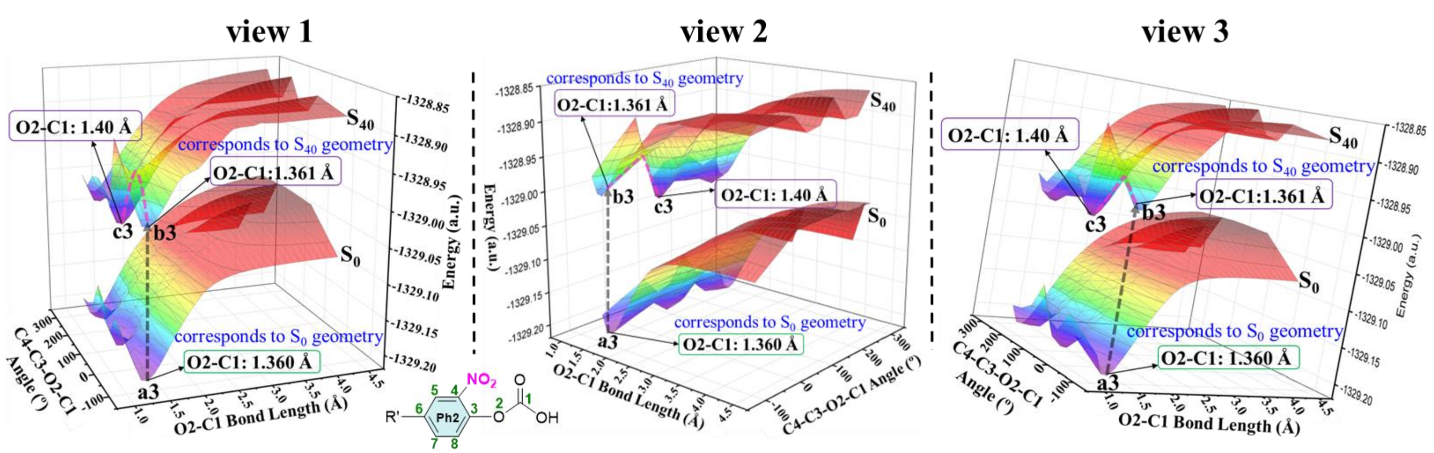

Fig. S12 Three different views of PES for *m*(NO_2)-BPAHC. (R'=HOPh(NO_2)C(CH_3)$_2$-)

To understand the substituent effect on carbonate PhO–COO bond, Fig. 6 displays the GS and ES PESs for BPAHC (Fig. 6 center), *m*(NH_2)-BPAHC (Fig. 6 left), and *m*(NO_2)-BPAHC (Fig. 6 right). Corresponding to these PESs in Fig. 6, the other three different views of PESs for each model are shown in Figs. S10, S11, and S12 for BPAHC, *m*(NH_2)-BPAHC, and *m*(NO_2)-BPAHC, respectively, in order to show the PESs more clearly.

2.8 Possible singlet-triplet intersystem crossing for BPAHC

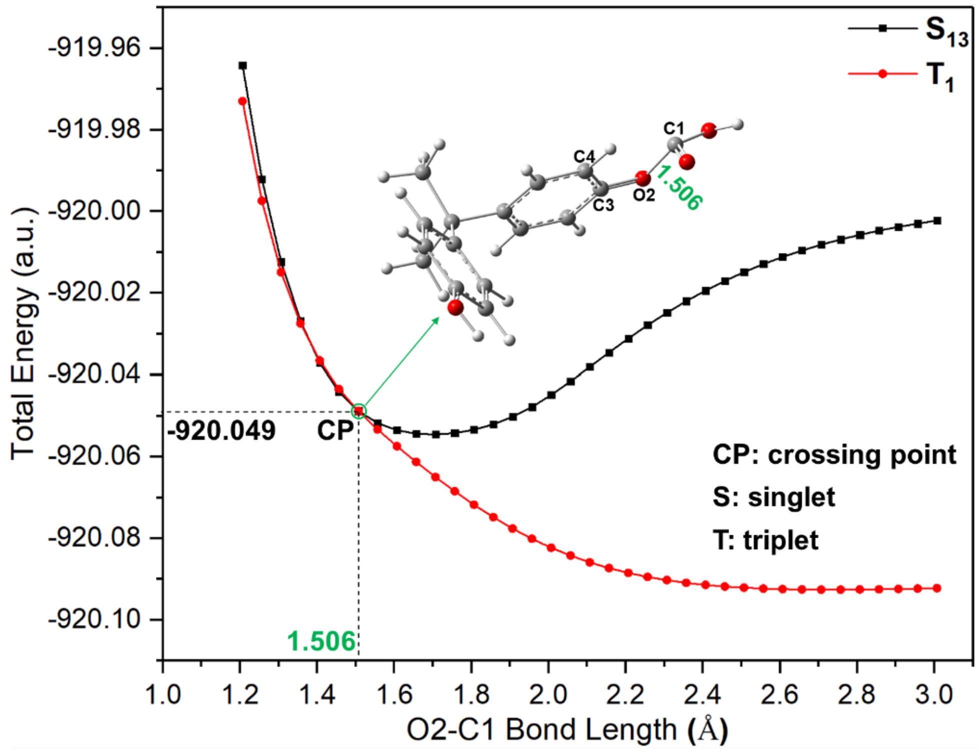

Fig. S13 Intersystem crossing from the excited singlet to triplet for BPAHC.

To examine whether the intersystem crossing exists or not between the excited singlet and triplet states, the crossing point (see Fig. S13) between the excited singlet and triplet states was obtained. According to the results as shown in Fig. S13, there is a high possibility to have the intersystem crossing from the excited singlet to triplet through a crossing point (O2-C1 bond length: 1.506 Å), finally getting the separated radicals Ph=O• and •COOH.

3. References

S1 A. Rivaton, J. Lemaire, *Polym. Degrad. Stabil.* 1988, **23**, 51-73.

S2 C. Y. Legault, CYLview, version 1.0b; Université de Sherbrooke: Sherbrooke, Quebec, Canada, 2009.

S3 T. Lu, F.W. Chen, *J. Comput. Chem.*, 2012, **33**, 580-592.

S4 E. Seifert, *J. Chem. Inf. Model.*, 2014, **54**, 1552-1552.

S5 Gaussian 16, Revision A.03, M. J. Frisch, G. W. Trucks, H. B. Schlegel, G. E. Scuseria, M. A. Robb, J. R. Cheeseman, G. Scalmani, V. Barone, G. A. Petersson, H. Nakatsuji, X. Li, M. Caricato, A. V. Marenich, J. Bloino, B. G. Janesko, R. Gomperts, B. Mennucci, H. P. Hratchian, J. V. Ortiz, A. F. Izmaylov, J. L. Sonnenberg, D. Williams-Young, F. Ding, F. Lipparini, F. Egidi, J. Goings, B. Peng, A. Petrone, T. Henderson, D. Ranasinghe, V. G. Zakrzewski, J. Gao, N. Rega, G. Zheng, W. Liang, M. Hada, M. Ehara, K. Toyota, R. Fukuda, J. Hasegawa, M. Ishida, T. Nakajima, Y. Honda, O. Kitao, H. Nakai, T. Vreven, K. Throssell, J. A. Montgomery, Jr., J. E. Peralta, F. Ogliaro, M. J. Bearpark, J. J. Heyd, E. N. Brothers, K. N. Kudin, V. N. Staroverov, T. A. Keith, R. Kobayashi, J. Normand, K. Raghavachari, A. P. Rendell, J. C. Burant, S. S. Iyengar, J. Tomasi, M. Cossi, J. M. Millam, M. Klene, C. Adamo, R. Cammi, J. W. Ochterski, R. L. Martin, K. Morokuma, O. Farkas, J. B. Foresman, and D. J. Fox, Gaussian, Inc., Wallingford CT, 2016.

S6 Y. Zhao, D. G. Truhlar, *Theor. Chem. Account*, 2008, **120**, 215-241.

S7 J. Chai, M. Head-Gordon, *Phys. Chem. Chem. Phys.*, 2008, **10**, 6615-6620.

S8 F. Weigend, R. Ahlrichs, *Phys. Chem. Chem. Phys.*, 2005, **7**, 3297-3305.

S9 D. Rappoport, F. Furche, *J. Chem. Phys.*, 2010, **133**, 134105.

S10 D. Jacquemin, B. Mennucci and C. Adamo, *Phys. Chem. Chem. Phys.*, 2011, **13**, 16987-16998.

4. Coordinates

m(NH_2)-BPAHC (S_0 geometry)

1	0	5.146392	-2.608699	0.433577
8	0	5.380008	-1.955503	-0.262523
6	0	4.375250	-1.044982	-0.213828
6	0	3.395903	-1.144743	0.794074
6	0	4.288607	-0.019924	-1.154309
6	0	2.343520	-0.235405	0.826842
6	0	3.228562	0.888487	-1.097295
6	0	2.230797	0.799841	-0.117216
1	0	1.585266	-0.341301	1.600238
1	0	3.188732	1.672265	-1.846132
6	0	1.067340	1.805007	0.002410
6	0	0.984459	2.756059	-1.216209
1	0	0.866483	2.208119	-2.156365
1	0	0.118600	3.417014	-1.105816
1	0	1.878457	3.385648	-1.292306
6	0	1.325754	2.681397	1.251921
1	0	0.570904	3.469577	1.353638
1	0	1.331930	2.089772	2.173217
1	0	2.303823	3.165029	1.160709
6	0	-0.273385	1.044777	0.088190
6	0	-0.566610	0.083082	-0.888095
6	0	-1.232619	1.303683	1.075996
6	0	-1.783379	-0.610215	-0.912897
1	0	0.172004	-0.144926	-1.652848
6	0	-2.450020	0.616737	1.083352
1	0	-1.049346	2.037715	1.851377
6	0	-2.717173	-0.318254	0.097024
8	0	-3.877713	-1.111449	0.084440
6	0	-5.089577	-0.527744	0.168634
8	0	-5.337217	0.643278	0.319163
8	0	-6.007573	-1.510177	0.064603
1	0	-6.871020	-1.068040	0.137443
7	0	-2.094933	-1.522585	-1.918508
1	0	-1.295224	-1.955269	-2.362611
1	0	-2.811876	-2.192520	-1.670363
1	0	-3.191580	0.815732	1.848104
7	0	3.571090	-2.245090	1.712256
1	0	3.971578	-1.930783	2.595710
1	0	2.683094	-2.691424	1.929968
1	0	5.044073	0.049810	-1.930814

m(NH_2)-BPAHC (S_{21} geometry)

1	0	-4.281074	-3.339334	0.883723
8	0	-4.812758	-2.524141	0.806058
6	0	-3.988396	-1.512294	0.448440
6	0	-2.752782	-1.750281	-0.168088
6	0	-4.373757	-0.191010	0.723852
6	0	-1.931278	-0.647174	-0.459203
6	0	-3.536893	0.912351	0.403734
6	0	-2.291049	0.712116	-0.152789
1	0	-0.966176	-0.819692	-0.925124
1	0	-3.885244	1.905990	0.653813
6	0	-1.318291	1.843707	-0.544910
6	0	-1.624645	3.143689	0.232440
1	0	-1.591302	3.001642	1.316368
1	0	-0.875359	3.895986	-0.027089
1	0	-2.608059	3.553642	-0.026804
6	0	-1.628310	2.125261	-2.046355
1	0	-0.933912	2.881951	-2.422797
1	0	-1.528693	1.235271	-2.674799
1	0	-2.651932	2.499017	-2.157687
6	0	0.149080	1.417947	-0.339308
6	0	0.711876	1.429420	0.964222
6	0	0.934518	0.925434	-1.373419
6	0	1.996555	0.952543	1.210809
1	0	0.134703	1.802664	1.807090
6	0	2.238158	0.429548	-1.135764
1	0	0.567770	0.898054	-2.394540
6	0	2.794351	0.418712	0.150117
8	0	3.987100	-0.039084	0.484111
6	0	4.679647	-1.232804	-0.579441
8	0	3.944230	-2.194711	-0.786558
8	0	5.919141	-1.374812	0.017379
1	0	5.964105	-2.319933	0.259272
7	0	2.593280	0.999936	2.468912
1	0	1.978008	0.853033	3.258730
1	0	3.430005	0.423039	2.486643
1	0	2.803591	0.016274	-1.958728
7	0	-2.371963	-3.064106	-0.434094
1	0	-3.026242	-3.615001	-0.981626
1	0	-1.417623	-3.188683	-0.752631
1	0	-5.316197	-0.035728	1.238526

m(NO_2)-BPAHC (S_0 geometry)

1	0	-5.262106	-2.079966	0.448563
8	0	-5.214421	-1.384140	1.148815
6	0	-4.197322	-0.580679	0.820332
6	0	-3.380160	-0.739723	-0.326623
6	0	-3.904497	0.502134	1.664217
6	0	-2.329093	0.144752	-0.599954
6	0	-2.863085	1.372701	1.379141
6	0	-2.047283	1.217599	0.239069
1	0	-1.737636	-0.044926	-1.487888
1	0	-2.682894	2.190642	2.067953
6	0	-0.915219	2.197684	-0.131444
6	0	-0.618367	3.207733	1.003741
1	0	-0.343884	2.709473	1.939064
1	0	0.218642	3.850133	0.712522
1	0	-1.481723	3.854545	1.195668
6	0	-1.373876	3.006263	-1.368548
1	0	-0.637404	3.770021	-1.643028
1	0	-1.548848	2.364360	-2.238112
1	0	-2.313942	3.518763	-1.141160
6	0	0.381772	1.408366	-0.399722
6	0	0.853379	0.519332	0.572803
6	0	1.150815	1.558901	-1.560196
6	0	2.040211	-0.190057	0.406115
1	0	0.296193	0.344831	1.485117
6	0	2.347574	0.862126	-1.730562
1	0	0.831545	2.229152	-2.350032
6	0	2.811661	-0.014262	-0.756841
8	0	3.977407	-0.694082	-1.045005
6	0	5.035883	-0.518502	-0.209175
8	0	5.103954	0.274816	0.694540
8	0	5.997975	-1.356659	-0.611068
1	0	6.745879	-1.216219	-0.004681
7	0	2.402954	-1.140309	1.470794
8	0	3.262909	-1.985273	1.227455
8	0	1.798410	-1.051134	2.537580
1	0	2.944811	0.989905	-2.627257
7	0	-3.607445	-1.828706	-1.255641
8	0	-4.542773	-2.625357	-1.014015
8	0	-2.887424	-1.935152	-2.241447
1	0	-4.519858	0.632040	2.548253

m(NO_2)-BPAHC (S_{40} geometry)

1	0	-5.336948	-2.006603	0.356856
8	0	-5.290393	-1.322229	1.068430
6	0	-4.248650	-0.536672	0.774438
6	0	-3.409149	-0.697960	-0.356109
6	0	-3.951688	0.527515	1.639935
6	0	-2.332871	0.166486	-0.593092
6	0	-2.885042	1.378668	1.390614
6	0	-2.046575	1.220928	0.267661
1	0	-1.724912	-0.023189	-1.469795
1	0	-2.702952	2.183425	2.094399
6	0	-0.888483	2.183327	-0.065015
6	0	-0.582898	3.158668	1.097865
1	0	-0.337168	2.630877	2.024908
1	0	0.276508	3.783217	0.834544
1	0	-1.430632	3.825460	1.291508
6	0	-1.319343	3.032441	-1.285352
1	0	-0.569291	3.793358	-1.528428
1	0	-1.490264	2.416765	-2.174362
1	0	-2.255628	3.551054	-1.055874
6	0	0.397574	1.374851	-0.339160
6	0	0.818442	0.438613	0.603444
6	0	1.190723	1.570706	-1.482429
6	0	2.017023	-0.290148	0.426959
1	0	0.223568	0.235577	1.486359
6	0	2.383542	0.857123	-1.664433
1	0	0.895742	2.281375	-2.244309
6	0	2.812992	-0.058037	-0.726622
8	0	3.969936	-0.786981	-0.968144
6	0	5.082054	-0.414320	-0.276870
8	0	5.159139	0.498400	0.505144
8	0	6.070087	-1.240766	-0.642230
1	0	6.850107	-0.970146	-0.127326
7	0	2.362122	-1.205649	1.374818
8	0	3.372412	-2.012773	1.396065
8	0	1.704316	-1.463374	2.461799
1	0	2.994168	1.012827	-2.547916
7	0	-3.639299	-1.768634	-1.305309
8	0	-4.597109	-2.547859	-1.095805
8	0	-2.900075	-1.877710	-2.276447
1	0	-4.584453	0.659165	2.511369